Mid-infrared absorption, emission, and non-linear response in extreme sub-wavelength lms

Zarko Sakotic , Amogh Raju , Wooje Chang[b], Alexander Ware , Felix Estevez Hilario , Madeline Brown , Divya Hungund , Yonathan Magendzo , Michelle Povinelli[c], Thomas Truskett[b], Delia Milliron[b], and Daniel Wasserman

Chandra Family Department of Electrical and Computer Engineering, University of Texas at Austin, Austin, Texas 78758, United States
[b]McKetta Department of Chemical Engineering, University of Texas at Austin, Austin, Texas 78712, United States
[c]Ming Hsieh Department of Electrical and Computer Engineering, University of Southern California, Los Angeles, California 90089, United States

ABSTRACT

We present an analytical formalism to predict the minimal thickness of a film, with an intrinsic absorption resonance, required to perfectly absorb all incident light. We show that on resonance, perfect absorption can be achieved at thicknesses well below one-thousandth of a free-space wavelength. The developed analytical formalism is validated numerically using rigorous coupled wave analysis and finite element techniques, and experimentally using thin-film superlattices of tin-doped indium oxide nanocrystals with collective plasmon resonances mimicking the absorption resonances considered in our analytical model. We further consider perfectly absorbing structures consisting of thin, non-resonant, but high loss, films, and show that perfect absorption can often only be achieved at film thicknesses well below what can be fabricated experimentally. We overcome this limitation by introducing the concept of thin-film dilution, and show, analytically, numerically, and experimentally, that these diluted films can accurately mimic the theoretical optical properties of nanometer, or even sub-atomic, thickness films. This work provides a path towards the rational design of ultra-thin absorbers for bolometric or non-linear optical applications.

Keywords: mid-infrared, thin film, perfect absorption, ITO, metamaterial, plasmonic, thermal emission

1. INTRODUCTION

The field of nanophotonics is, at its core, centered around the design and demonstration of photonic structures capable of confining light down to the nano-scale. Reducing the dimensions of optical and opto-electronic structures and devices offers the pragmatic benefits typically associated with device scaling, such as increased device density and decreased power requirements. More fundamentally, achieving such structures and devices also offers opportunities to enhance the interaction between optical fields and nano-scaled matter, such as sub-cellular components, molecules, and/or electronic devices. The primary challenge of nanophotonics is not related to any intrinsic properties of the nanoscale, but more that such lengths scales are almost always below the diffraction limit for much of the electromagnetic spectrum. At the longer wavelengths of the mid-infrared (mid-IR, $\lambda = 2 \quad 30$ m) the discrepancy between the nano-scale and optical wavelengths is even starker, and bridging that gap even more challenging.

In the vast majority of nanophotonic applications, loss (either via scattering mechanisms or material absorption) is highly detrimental to the efficient operation of nanophotonic devices or structures. Loss is also largely unavoidable, particularly when attempting to operate below the diffraction limit.[1] Yet there does exist a sub-field of nanophotonics, focused on the design and demonstration of 'perfect absorption' where loss is not

Further author information: (Send correspondence to D.W.)
D.W.: E-mail: dw@utexas.edu

Active Photonic Platforms (APP) 2024, edited by Ganapathi S. Subramania, Stavroula Foteinopoulou, Proc. of SPIE Vol. 13110, 131100F
 · 0277-786X · doi: 10.1117/12.3025541

only acceptable, but in fact the primary objective. Cynically, one could argue that demonstrations of perfect absorption are so ubiquitous in part because loss is (relatively) easy to achieve in nanophotonic structures. A kinder interpretation would note that perfect absorption has a number of viable applications, and more fundamentally, does fall into the general category of enhanced light matter interaction, so that the extremes of perfect absorption may offer insight into the ultimate limits of such interactions.

Demonstrations of enhanced absorption can take many forms. Absorption can be achieved in carefully engineered metamaterial structures,[2 3] thin metallic, plasmonic, or phononic films,[4–6] or more recently a range of 2D materials.[7–9] Clearly, the demonstration of absorption enhancement in photodetector architectures has very real applications for solar energy harvesting, optical communication, and imaging, to name only a few applications.[10–15] The enhanced transduction of electromagnetic energy to electrical signals (traditional photon detection) is a vital, far-ranging, and extensive field of research, but ultimately not the subject of this work. Here, when we speak of enhanced, or perfect, absorption, we are only referring to the transduction of electromagnetic energy to heat. Even with this more limited scope, there exist a wide range of potential applications. First and foremost is the bolometer,[16] a device which absorbs incident radiation and thus heats up the absorbing element, whose temperature change is read out, typically in the element's change of resistance. The lower the thermal mass of a bolometric element, the larger the element's temperature change with absorbed energy, and thus the more efficient the detection of radiation. Perfect absorbers can also be used as chemical sensors, where the presence of a molecular absorption feature or a refractive index change can be read out in the change of the spectral response of the absorber.[17 18] Absorption also has vital medical/health applications, particularly for photothermal cancer therapy, where absorbing nanoparticles are functionalized to bind to cancerous cells, and when irradiated at their absorption resonance, undergo a significant temperature change, with the goal of ablating the attached cancerous cells.[19–21] Kirchoff's Law states that the absorptivity of a surface is equivalent to its emissivity; thus designing a thin film with spectrally or angularly selective absorption, particularly at thermal wavelengths, can result in selective thermal emitters for IR sensing or signalling applications.[22–24] Very different mechanisms can even be leveraged in the same structure, to enhance absorption at one wavelength and angle of incidence, while promoting thermal emission at very different wavelengths and angles.[25]

Many, if not all, of the applications for selective and strong absorption could be enhanced by the reduction of the absorbing volume. This raises the rather intriguing question of what the ultimate size limit is at which perfect absorption can be achieved. There have been a number of studies investigating the limit of absorption in solar cells, which has very obvious and important implications for the larger field of solar energy harvesting.[26 27] More fundamental, and quite comprehensive, investigations of absorption in structured systems have also been published.[28] Here we focus on the fundamental thickness limit in ultra-thin, planar, absorbing films, in the tradition of early work on thin metal films for radar applications.[29 30]

2. THE ULTIMATE THICKNESS LIMITS FOR RESONANTLY ABSORBING THIN FILMS

Here we consider a thin film of thickness t with a resonant absorption feature, such as polar dielectric's absorption at the transverse optical (TO) phonon energy. The absorption of such a film can be modeled quite accurately with a Lorentzian lineshape, as shown in Fig. 1a. We consider two cases: in the first, the absorbing thin film is free-standing, surrounded on either side by vacuum, in the second, the thin film is held above a perfectly reflecting mirror (either a perfect electrical conductor, PEC, or perfect magnetic conductor, PMC) with a dielectric spacer thickness of d. Both configurations are shown schematically in Fig. 1b and c. We can model either system using a transmission line model, where the absorbing thin film is described by a complex sheet conductivity:[31]

$$\sigma^s = \sigma^s_{Re} + i\sigma^s_{Im} = Y_o \frac{i2\pi t\,(\ (\lambda)\quad 1)}{\lambda} \quad , \qquad (\lambda) = \quad + i \tag{1}$$

For such a system, the impedance of the thin film is simply $Z_s = 1/\sigma^s$, and the maximum absorption condition can be found by searching for the reflection zero (in the case of the mirror-backed system) or the minima of the sum of reflection and transmission (for the free-standing thin film), of the transmission line model of the optical system. This results in a maximum absorption of $A = 50\%$ for the free-standing thin-films and

perfect absorption ($A = 100\%$) for the mirror-backed films. The film thickness resulting in such absorption is $t_w = \lambda_o/\pi$ for the free-standing film and $t_w = \lambda_o/2\pi$ for the mirror-back configuration. We dub the thickness of maximum absorption (t_W) the 'resonant' Woltersdorff thickness, to recognize Woltersdorff's original derivation of maximum absorption thickness for a free-standing metal film.[29] Interestingly, t_W for both configurations depends only on the imaginary part of the complex conductivity (as long as > 5). Figure 1(d) shows the calculated mirror-backed resonant Woltersdorff thicknesses for a number of materials with resonant absorption features. In almost all cases, perfect absorption can be achieved in thicknesses well under one thousandth of a free space wavelength. In the case where the thin-film absorber is embedded in a cavity, we derive the cavity-enhanced resonant Woltersdorff thickness to be $t_w = (\lambda_o/4)(1/Q)$, where Q is the quality factor of the cavity. Embedding a thin film with an intrinsic absorption resonance in a cavity can, for cavities of even moderate Q, reduce the required absorber thickness well below a monolayer, a result that is clearly un-physical. Later in this proceedings we will show that absorbing films with un-physical thicknesses can be mimicked using the concept of geometric dilution. Detailed derivations, absorption spectra, and numerical validation of our analytical perfect absorption framework are presented in greater depth in Ref. 32.

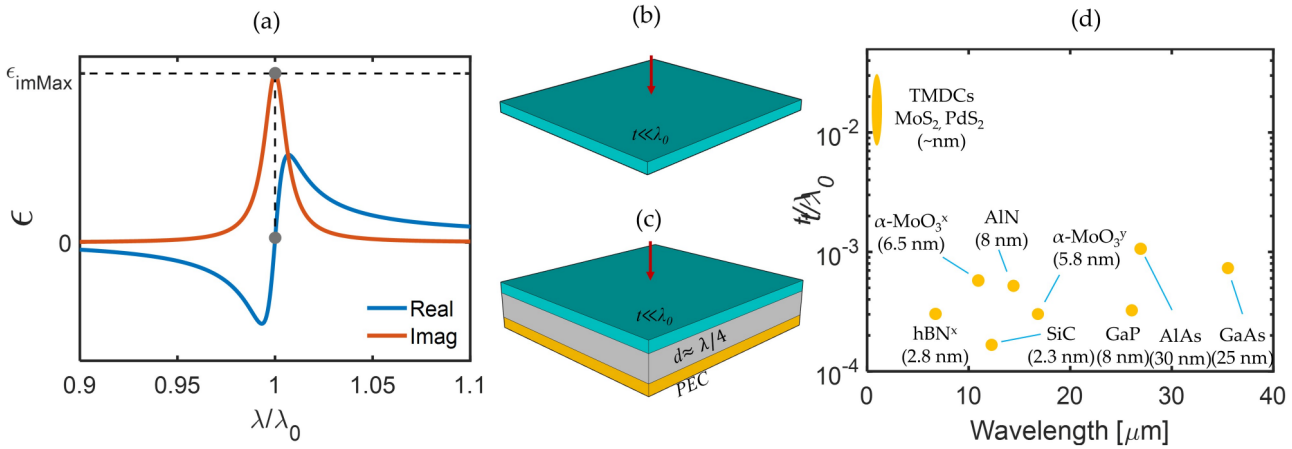

Figure 1. (a) Real (blue) and imaginary (red) permittivity associated with a Lorentzian absorption feature such as what might be observed in a polar dielectric with a transverse optical phonon resonance at λ . Schematics of the (b) free-standing and (c) PEC mirror-backed configurations considered in this work. (d) Calculated resonant Woltersdorff thickness for perfect absorption in PEC mirror-backed configurations for a variety of polar dielectric and 2D materials.

3. INFRARED PERFECT ABSORPTION WITH TIN DOPED INDIUM OXIDE NANOCRYSTAL SUPERLATTICES

The analytical formalism described in Section 2 and Ref. 32 assumes a thin film with a Lorentzian absorption (and the corresponding complex permittivity). Such absorption spectra are excellent representations of the optical response of a wide array of polar dielectrics in the vicinity of their optical phonon energies, as well as 2D materials' exciton absorption features. However, in each of these cases, the absorption feature is spectrally fixed to the energy of the material resonance, and is not in and of itself, design-able. A thin-film material system having an absorption resonance with controllable spectral position and amplitude would offer an ideal system to experimentally validate the analytical formalism developed in Section 2.

To this end, we consider the recently developed and demonstrated tin-doped indium oxide (ITO) nanocrystal (NC) superlattice thin film system. Indium oxide (In_2O_3) is a wide band gap semiconductor which can be synthesized in NC form with controllable NC diameter. When tin is incorporated into the indium oxide synthesis, ITO NC's are formed heavily doped with free carriers, to the point where they are able to support localized surface plasmon resonances (LSPRs) in the mid-infrared.[33–35] Using a liquid-air interface technique, 2D arrays (superlattices) of doped ITO NC monolayers can be deposited on a wide array of surfaces. The formation of the superlattice results in an optical response best described as a collective plasmonic response (CPR), whose effective permittivity can be modelled accurately with a Lorentzian absorption. Control of NC doping and diameter allow

for independent control of the absorption spectral position and amplitude, respectively.[36] Thus, doped ITO NC superlattice films offer an ideal material system to experimentally validate the analytical formalism of Section 2.

We begin our investigation by fabricating the base quarter-wave cavity required for the mirror-back configuration shown in Fig. 1a. An optically-thick ($\sim$ 78 nm layer of Au is deposited on a Si wafer with a thin ($\sim$ 5 nm layer of Ti for adhesion. Above the Au we deposit a 195 nm layer of Ge by e-beam evaporation. Here, the Au, which is highly reflective across the mid-IR, serves as our perfect electrical conductor (PEC) and the Ge film serves as our lossless dielectric spacer. The large refractive index of Ge ($n_{Ge} \approx 4$) allows us to grow relatively thin layers of the dielectric spacer while still achieving optical thicknesses of a quarter wavelength. Upon the Ge surface, we use a modified liquid-air interface technique to assemble the ITO NC monolayers.[37] The resulting thin film systems are characterized by reflection spectroscopy in an IR microscope coupled to a Fourier transform infrared (FTIR) spectrometer. Because the bottom Au mirror is nearly perfectly reflecting (and allows no transmission), absorption of the thin film can be determined simply by $A(\lambda) = 1 \quad R(\lambda)$, where $R(\lambda)$ is the measured spectral reflectivity of the system. The system is simulated by first modeling the ITO superlattice thin film permittivity using the mutual polarization method (MPM),[36 38] resulting in a imaginary part of the permittivity very closely resembling that of a Lorentzian absorption function. The total reflectivity (or absorption) of the system can be modeled, using the MPM-calculated permittivity, by either a transmission line transfer matrix method, or alternatively, by rigorous coupled wave analysis or finite element methods.

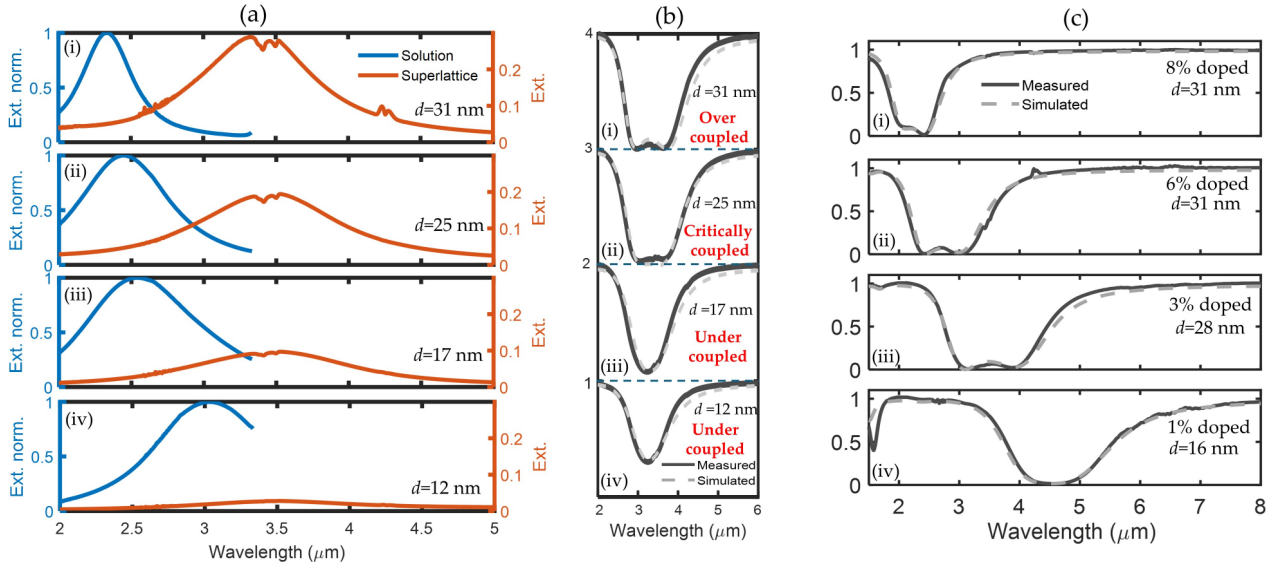

Figure 2. (a) Measured experimental extinction of tin-doped indium oxide nanocrystals in solution (dashed) and in monolayer superlattice formation (solid) for NC diameters and doping (% Sn): i) $d = 31$ nm and doping 3.0% Sn , ii) $d = 25$ nm and doping 2.7% Sn, iii) $d = 17$ nm and doping 2.5% Sn , iv) $d = 12$ nm and doping 2.2% Sn. (b) Experimental (solid) and simulated (dashed) reflection spectra for the ITO NC superlattices of (a) on a leaky cavity comprising Ge deposited above a Au mirror. (c) Experimental (solid) and simulated (dashed) reflection spectra for samples with doping and diameter chosen to shift perfect absorption feature across the mid-IR. i) $d = 16$ nm and doping 8% Sn, ii) $d = 28$ nm and doping 6% Sn, iii) $d = 31$ nm and doping 3% Sn, and iv) $d = 31$ nm and doping 1% Sn.

Increasing the thickness of the ITO NCs increases the amplitude of the absorption feature, without tuning the resonant wavelength of an individual NC's LSPR. However, the spacing of NCs, which is determined by the size of the oleate ligands on the NCs, remains constant; the larger diameter NC superlattices have larger filling fractions and thus larger redshifts from the individual NC LSPRs. In this work we investigate a series of ITO monolayers with NC diameters of 12, 17, 25, and 31 nm. The Sn fraction of these NCs superlattices were thus tuned from 2.2, 2.5, 2.7, to 3% with increasing diameter to keep the CPR at $\lambda = 3.4$ m, but allow for increasing absorption amplitude. The experimentally measured extinction coefficients for the four different monolayers (deposited on Si wafers to avoid cavity effects) are shown in Fig. 2a, and indeed show the expected increase in absorption with increasing NC diameter. The reflection from this set of samples is presented in Fig.

2b, and clearly shows absorption features indicative of an undercoupled ($D = 12\,\text{nm}$ and $D = 17\,\text{nm}$ NCs), nearly critically coupled ($D = 25\,\text{nm}$ NCs), and overcoupled ($D = 31\,\text{nm}$) system. For the nearly critically coupled system ($D = 25\,\text{nm}$), reflectively of less than a few percent is observed on resonance. For the overcoupled system ($D = 31\,\text{nm}$), the so-called Rabi splitting of the reflection feature, typically associated with strong coupling, is observed.

By controlling the dielectric spacer thickness and the NC diameter and doping, perfect absorption can be achieved across the infrared spectral range. This can be seen in Fig. 2c, where combinations of doping and NC diameter are utilized to demonstrate, experimentally, strong absorption features ranging from $\lambda < 2$ m to $\lambda = 4.6$ m. The ITO NC 2D superlattices offer a flexible, low-cost, and large area implementation of the analytical framework developed in this work to predict and design perfect absorption in the minimal thickness possible for a thin film with a resonant absorption feature. Notably, we demonstrate perfect absorption in films of thickness less than one hundredth of a free space wavelength. Moreover, the field profile, on resonance, in the NC superlattice suggests that the remarkable vertical confinement of energy in the three-layer system is complemented by a lateral field concentration in the regions between adjacent NCs. This 3D field concentration has significant implications not only for ultra-thin, low thermal mass bolometric elements, but also for strongly enhanced nonlinear response in ITO NC superlattices. Details of the modeling, synthesis and fabrication, and characterization of the thin film ITO NC perfectly absorbing films can be found in the main text and supplementary information of Ref. 39.

4. PERFECT ABSORPTION IN THIN FILMS WITHOUT RESONANT ABSORPTION FEATURES

Both our analytical framework and the experimental validation of the developed framework assumed a thin film absorber with a resonant absorption feature. However, perfect absorption should still be possible even without a resonant absorption feature, as long as the imaginary component of the absorber's permittivity is suitably large. Assuming this condition is met (ie a lossy thin film), the Woltersdorff condition $t_W = \lambda_0/2\pi$ can be applied and a minimal thickness required to achieve perfect absorption calculated. Here we consider metals as our non-resonant lossy films, as most metals have large losses ($\gg 1$) across the mid-IR. We can plot the minimal thickness for perfect absorption across the mid-IR for a number of typical metals, using permittivity values from the literature (Fig. 3a). What becomes clear is that achieving perfect absorption in a planar metal film, particularly as one moves to longer wavelengths, requires extremely thin metal films. In fact, the thicknesses required are extremely difficult to achieve with traditional fabrication techniques, being below the typical percolation threshold for planar metal films.[40] The island-like growth of sub-percolation threshold metal films, not surprisingly, leads to significant uncertainty and variation in film permittivity (with significant dependence on growth parameters and film morphology), making such films unreliable components in deterministic designs for perfect absorption.[41] There has been significant effort, in recent years, to develop techniques capable of providing high quality, ultra-thin, metal films. Such efforts include epitaxial growth of crystalline metal films[42] or growth mechanisms promoting percolation at reduced thicknesses in order to achieve high quality planar metals with thicknesses below 10 nm.[43] [44]

However, achieving consistent and repeatable optical properties in such thin film metals, and with optical properties comparable to bulk metals, is very challenging. Thus, in order to achieve perfect absorption in non-resonant, highly lossy, thin films, one must either develop an approach to producing high quality, planar films with reproducible optical properties, or alternatively, find some way to mimic such behavior. Figure 3b shows the simulated spectral response for for a Au metal film deposited upon a Ge spacer and Au backing mirror, as a function of the top Au layer's thickness. As can be seen here, changing the metal thickness, but assuming the film retains the optical properties of a bulk layer of Au, shifts the spectral response of the system. Alternatively, one could analytically 'dilute' a Au film of constant (30 nm) thickness, writing its permittivity as $_{dilute} = f * \quad _{ir} + (1 \quad f) * \quad _{u}$, where f is an analytical filling factor, a measure of the dilution of the top metal film (Fig. 3c). Simulated reflection spectra for a planar top Au film, assuming bulk permittivity, with thicknesses $t = 30$, 15, 7.5, 3.75, and 0 nm are shown in Fig 3d. Simulated reflection spectra of analytically diluted Au top layers with varying analytical dilution fill factors effectively mimicking the varying thicknesses shown in Fig 3d are shown in Fig 3e.

It turns out that the same effect can be achieved by physically removing a fraction of the top film, as long as the holes patterned into the film are well below a wavelength in scale. Figure 4a shows the simulated optical response of a system with a geometrically diluted film, as modeled using rigorous coupled wave analysis. Excellent match is seen for each of the simulated systems: ideal Au film of varying thickness (Fig. 3b), analytically diluted thin film (Fig. 3c), and a geometrically diluted thin film (Fig. 4a). Note that the extraneous features seen in the geometrically diluted thin film are a result of simulation artifacts.

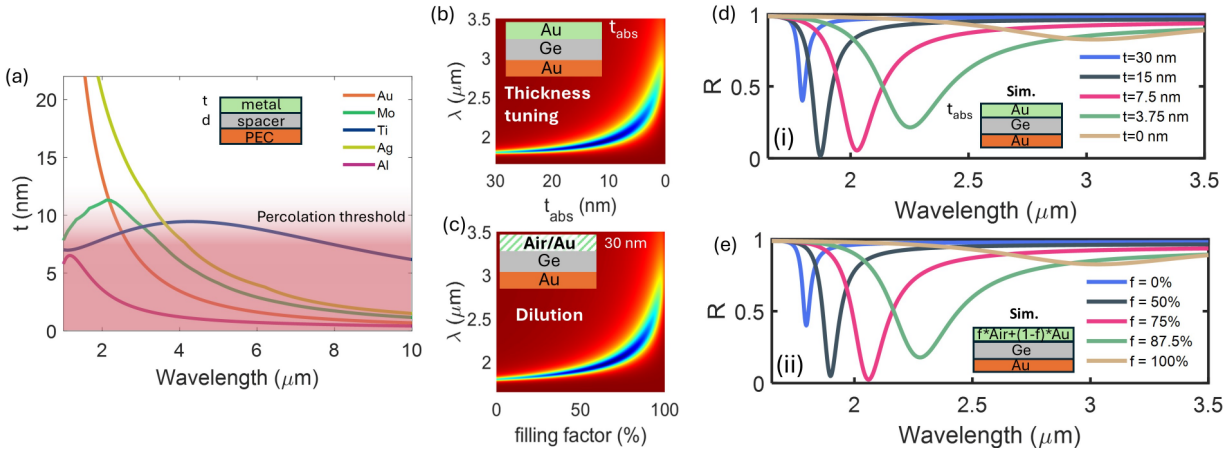

Figure 3. (a) Thickness required to achieve perfect absorption for thin metal films suspended over a PEC, as a function of mid-IR wavelength. The approximate thickness regime where typical metal films have their percolation thickness is shaded red. Simulated reflection for (b) a thin metal Au film deposited on 150 nm of Ge above a Au mirror, assuming bulk optical properties for the Au, and (c) for an analytically diluted Au film, where $_{dilute} = f * \ _{ir} + (1 \ \ f) * \ _{u}$, with f as being the analytical fill factor. Simulated reflection spectra of (d) the system in (b) for varying thicknesses of Au and (e) the system of (c) for varying fill factors f.

To experimentally demonstrate the concept of geometric dilution, a sample is fabricated comprising a Au mirror, above which is grown 150 nm of Ge. A top patterned layer of Au (30 nm) is then fabricated by e-beam lithography, metallization, and lift-off. The patterned Au comprises a number of patterns, all square arrays of square apertures with periodicity $\ = 400$ nm, and aperture widths $w = 0$, 200, 300, 350 and 400 nm, where $w = 0$ corresponds to a planar Au film and $w = 400$ nm corresponds to a bare Ge surface. Figure 4b show the experimental (and simulated) reflection spectra for the fabricated samples with geometrically diluted top Au films. These results clearly demonstrate that the geometric dilution of thin metal films, assuming that the films can be patterned with subwavelength scales, offers a mechanism to not only mimic the performance of much thinner metal films, but to do so while retaining the metal films' bulk optical properties, something not achievable in most experimentally-demonstrated ultra-thin metal films.

The thin, or geometrically diluted, metal films patterned above the dielectric surface allow tuning of the top layer's sheet conductivity to achieve impedance matching, and thus perfect absorption. Interestingly, when these same diluted films are placed within the dielectric spacer, they can have a very different effect on the overall behavior of the optical system. Specifically, these patterned films can introduce a phase shift for light propagating in the cavity, providing significant phase accumulation in minimal thicknesses. We refer to such layers as 'phase doping' of the cavity, effectively shrinking the round-trip for light in the cavity and allowing for tuning of the spectral position of perfect absorption. Combining phase doping layers in the cavity and the geometrically diluted absorbing layers on the cavity surface provides mechanisms for independently tuning phase and amplitude of the optical system. One could thus envision a system comprising a uniform layer stack (bottom mirror, dielectric, phase doping layer, dielectric, and diluted top metal film), but with an array of 'pixels' with very different absorption features (in terms of absorption amplitude or spectral position) determined solely by the geometry of the two uppermost (patterned) metal films. Details of the analytical, numerical, and experimental exploration of diluted metal absorbers and phase doping layers are presented in Ref. 45.

The perfect absorption of light in thin metal films patterned with subwavelength geometries has a number of

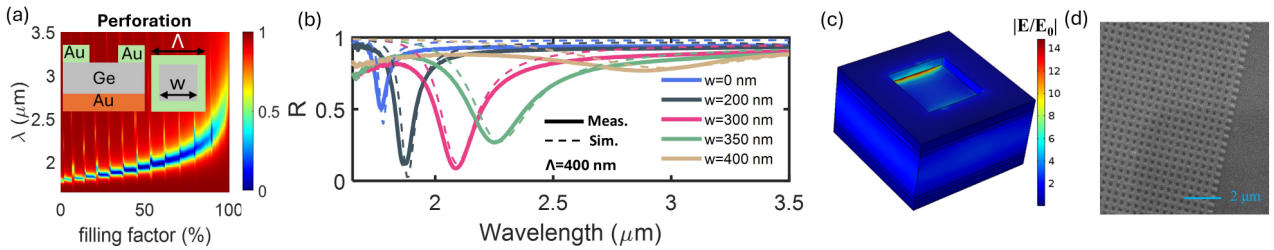

Figure 4. (a) Simulated reflection of a geometrically diluted film with square apertures of width w patterned into a $t = 30$ nm thick Au film for varying fill factor $f = w/$ for $= 400$ nm. (b) Experimental (solid) and simulated (dashed) reflection spectra of geometrically diluted thin film for varying aperture dimension (w) and constant period $= 400$ nm. (c) 3D plot of localized field, on resonance, of perfect absorber with geometrically diluted Au film. (d) Scanning electron micrograph of a diluted Au film.

potentially impactful applications. Of course, the reduced mass of the absorbing layer has implications for thin-film bolometric structures, where the underlying dielectric is replaced by an airgap and the metal film is effectively 'floated' on a supporting thin film over the mirror. Alternatively, the phase-doping and diluted metal absorber concept could be used to demonstrate spectral and spatial control over thermal emission from the multilayered stack. Of additional potential interest is the strong lateral field confinement in the diluted metal absorbers. The reduction in absorber volume achieved by the film dilution, while maintaining strong absorption, means that light is now absorbed in not only a limited vertical space, but limited lateral dimensions as well. Figure 4d shows an SEM of a patterned top Au layer, and Fig. 4c shows the simulated field profile for such an absorber. A strong lateral localization and enhancement of electrical field is observed in these simulations, suggesting that the proposed geometries could have significant application for engineering and enhancing nonlinear optical response.

5. CONCLUSION

In this work we describe an analytical approach to determine the minimum thickness of a resonantly absorbing thin film required to perfectly absorb all incident light. We dub this thickness the resonant Woltersdorff thickness, and show that for a range of polar dielectrics and 2D materials, this thickness is on the order of thousandths of a wavelength (or less). Monolayer 2D superlattices of plasmonic tin-doped indium oxide nanocrystals serve as an ideal experimental test system to validate our analytical formalism, with control of NC diameter and doping allowing for perfect absorption across a wide range of infrared wavelengths. In addition to the ITO NC material system, we show that perfect absorption can be achieved in planar, non-resonant, lossy thin films. However, experimental realization of metals thin enough to demonstrate perfect absorption at long wavelengths is extremely challenging. To overcome this, we show that geometric dilution of thin metal films allows us to mimic the behavior of much thinner metals (while maintaining the optical properties of bulk metal films). With this approach we can engineer perfect absorbers across the mid-IR with the same vertical stack, but different dilution factors. This work offers a variety of paths towards large area, low-cost, and ultra-low thermal mass perfect absorbers, thermal emitters, and non-linear optical systems for infrared source, sensor, and ultra-fast applications.

ACKNOWLEDGMENTS

The authors would like to acknowledge support from the Defense Advanced Research Projects Agency (DARPA) under the Optomechanical Thermal Imaging (OpTIm) program (HR00112320022) and the Air Force Office of Scientific Research (AFOSR) un der the Multidisciplinary University Research Initiative (MURI), Award No. FA9550-22-1-0307. Partial funding was provided by the Center for Dynamics and Control of Materials: an NSF MRSEC under Cooperative Agreement No. DMR-2308817. This work was also supported by the Welch Foundation (Grant Nos. F-1696 and F-1848).

REFERENCES

[1] Khurgin, J. and Boltasseva, A., "Reflecting upon the losses in plasmonics and metamaterials," *MRS Bulletin* **37** (08 2012).

[2] Landy, N. I., Sajuyigbe, S., Mock, J. J., Smith, D. R., and Padilla, W. J., "Perfect metamaterial absorber," *Phys. Rev. Lett.* **100**, 207402 (2008).

[3] Ra'di, Y., Simovski, C. R., and Tretyakov, S. A., "Thin perfect absorbers for electromagnetic waves: theory, design, and realizations," *Phys. Rev. Appl.* **3**, 037001 (2015).

[4] Li, Z., Butun, S., and Aydin, K., "Large-area, lithography-free super absorbers and color filters at visible frequencies using ultrathin metallic films," *Acs Photonics* **2**(2), 183–188 (2015).

[5] Nordin, L., Dominguez, O., Roberts, C., Streyer, W., Feng, K., Fang, Z., Podolskiy, V., Hoffman, A., and Wasserman, D., "Mid-infrared epsilon-near-zero modes in ultra-thin phononic films," *Appl. Phys. Lett.* **111**, 091105 (2017).

[6] Streyer, W., Law, S., Rooney, G., Jacobs, T., and Wasserman, D., "Strong absorption and selective emission from engineered metals with dielectric coatings," *Opt. Express* **21**, 9113 (2013).

[7] Li, Q., Lu, J., Gupta, P., and Qiu, M., "Engineering optical absorption in graphene and other 2d materials: advances and applications," *Advanced Optical Materials* **7**(20), 1900595 (2019).

[8] Epstein, I., Terrés, B., Chaves, A. J., Pusapati, V.-V., Rhodes, D. A., Frank, B., Zimmermann, V., Qin, Y., Watanabe, K., Taniguchi, T., et al., "Near-unity light absorption in a monolayer ws2 van der waals heterostructure cavity," *Nano letters* **20**(5), 3545–3552 (2020).

[9] Piper, J. R. and Fan, S., "Total absorption in a graphene monolayer in the optical regime by critical coupling with a photonic crystal guided resonance," *Acs Photonics* **1**(4), 347–353 (2014).

[10] Kamboj, A., Nordin, L., Petluru, P., Muhowski, A., Woolf, D., and Wasserman, D., "All-epitaxial guided-mode resonance mid-wave infrared detectors," *Applied Physics Letters* **118**(20) (2021).

[11] Pala, R. A., White, J., Barnard, E., Liu, J., and Brongersma, M. L., "Design of plasmonic thin-film solar cells with broadband absorption enhancements," *Adv. Mater* **21**(34), 3504–3509 (2009).

[12] Nordin, L., Petluru, P., Kamboj, A., Muhowski, A. J., and Wasserman, D., "Ultra-thin plasmonic detectors," *Optica* **8**(12), 1545–1551 (2021).

[13] Akhlaghi, M. K., Schelew, E., and Young, J. F., "Waveguide integrated superconducting single-photon detectors implemented as near-perfect absorbers of coherent radiation," *Nature communications* **6**(1), 8233 (2015).

[14] Tang, X., Ackerman, M. M., Shen, G., and Guyot-Sionnest, P., "Towards infrared electronic eyes: flexible colloidal quantum dot photovoltaic detectors enhanced by resonant cavity," *Small* **15**, 1804920 (2019).

[15] Li, W. and Valentine, J., "Metamaterial perfect absorber based hot electron photodetection," *Nano Lett.* **14**, 3510 (2014).

[16] Langley, S. P., "The bolometer and radiant energy," in [*Proceedings of the American Academy of Arts and Sciences*], **16**, 342–358, JSTOR (1880).

[17] Liu, N., Mesch, M., Weiss, T., Hentschel, M., and Giessen, H., "Infrared perfect absorber and its application as plasmonic sensor," *Nano Lett.* **10**, 2342 (2010).

[18] Mason, J. A., Allen, G., Podolskiy, V. A., and Wasserman, D., "Strong coupling of molecular and mid-infrared perfect absorber resonances," *IEEE Photonics Technol. Lett.* **24**, 31 (2012).

[19] Hirsch, L. R., Stafford, R. J., Bankson, J., Sershen, S. R., Rivera, B., Price, R., Hazle, J. D., Halas, N. J., and West, J. L., "Nanoshell-mediated near-infrared thermal therapy of tumors under magnetic resonance guidance," *Proceedings of the National Academy of Sciences* **100**(23), 13549–13554 (2003).

[20] Loo, C., Lowery, A., Halas, N., West, J., and Drezek, R., "Immunotargeted nanoshells for integrated cancer imaging and therapy," *Nano letters* **5**(4), 709–711 (2005).

[21] Stern, J. M., Stanfield, J., Kabbani, W., Hsieh, J.-T., and Cadeddu, J. A., "Selective prostate cancer thermal ablation with laser activated gold nanoshells," *The Journal of urology* **179**(2), 748–753 (2008).

[22] Greffet, J.-J., Carminati, R., Joulain, K., Mulet, J.-P., Mainguy, S., and Chen, Y., "Coherent emission of light by thermal sources," *Nature* **416**, 61 (2002).

[23] Liu, X., Tyler, T., Starr, T., Starr, A. F., Jokerst, N. M., and Padilla, W. J., "Taming the blackbody with infrared metamaterials as selective thermal emitters," *Physical review letters* **107**(4), 045901 (2011).

[24] Mason, J. A., Smith, S., and Wasserman, D., "Strong absorption and selective thermal emission from a midinfrared metamaterial," *Appl. Phys. Lett.* **98**, 241105 (2011).

[25] Ware, A., Bergthold, M., Mansfield, N., Sakotic, Z., Scott, E. A., Harris, C. T., and Wasserman, D., "Decoupling absorption and radiative cooling in mid-wave infrared bolometric elements," *Optics Letters* **48**(12), 3155–3158 (2023).
[26] Tiedje, T., Yablonovitch, E., Cody, G. D., and Brooks, B. G., "Limiting efficiency of silicon solar cells," *IEEE Transactions on electron devices* **31**(5), 711–716 (1984).
[27] Yu, Z., Raman, A., and Fan, S., "Fundamental limit of nanophotonic light trapping in solar cells," *Proceedings of the National Academy of Sciences* **107**(41), 17491–17496 (2010).
[28] Miller, O. D., Polimeridis, A. G., Homer Reid, M., Hsu, C. W., DeLacy, B. G., Joannopoulos, J. D., Soljačić, M., and Johnson, S. G., "Fundamental limits to optical response in absorptive systems," *Optics express* **24**(4), 3329–3364 (2016).
[29] Woltersdorff, V., "The optical constants of thinner metal layers in the infrared long wavelength," *Zeitschrift fur Phys* **91**, 230–252 (1934).
[30] Rozanov, K. N., "Ultimate thickness to bandwidth ratio of radar absorbers," *IEEE Transactions on Antennas and Propagation* **48**(8), 1230–1234 (2000).
[31] Li, Y. and Heinz, T. F., "Two-dimensional models for the optical response of thin films," *2D Materials* **5**(2), 025021 (2018).
[32] Sakotic, Z., Ware, A., Povinelli, M., and Wasserman, D., "Perfect absorption at the ultimate thickness limit in planar films," *ACS Photonics* **10**(12), 4244–4251 (2023).
[33] Kanehara, M., Koike, H., Yoshinaga, T., and Teranishi, T., "Indium tin oxide nanoparticles with compositionally tunable surface plasmon resonance frequencies in the near-ir region," *Journal of the American Chemical Society* **131**(49), 17736–17737 (2009).
[34] Jansons, A. W. and Hutchison, J. E., "Continuous growth of metal oxide nanocrystals: Enhanced control of nanocrystal size and radial dopant distribution," *ACS nano* **10**(7), 6942–6951 (2016).
[35] Staller, C. M., Gibbs, S. L., Saez Cabezas, C. A., and Milliron, D. J., "Quantitative analysis of extinction coefficients of tin-doped indium oxide nanocrystal ensembles," *Nano Letters* **19**(11), 8149–8154 (2019).
[36] Kim, K., Sherman, Z. M., Cleri, A., Chang, W. J., Maria, J.-P., Truskett, T. M., and Milliron, D. J., "Hierarchically doped plasmonic nanocrystal metamaterials," *Nano Letters* **23**(16), 7633–7641 (2023). PMID: 37558214.
[37] Bigioni, T. P., Lin, X.-M., Nguyen, T. T., Corwin, E. I., Witten, T. A., and Jaeger, H. M., "Kinetically driven self assembly of highly ordered nanoparticle monolayers," *Nature materials* **5**(4), 265–270 (2006).
[38] Sherman, Z. M., Kim, K., Kang, J., Roman, B. J., Crory, H. S. N., Conrad, D. L., Valenzuela, S. A., Lin, E., Dominguez, M. N., Gibbs, S. L., Anslyn, E. V., Milliron, D. J., and Truskett, T. M., "Plasmonic response of complex nanoparticle assemblies," *Nano Letters* **23**(7), 3030–3037 (2023). PMID: 36989531.
[39] Chang, W. J., Sakotic, Z., Ware, A., Green, A. M., Roman, B. J., Kim, K., Truskett, T. M., Wasserman, D., and Milliron, D. J., "Wavelength tunable infrared perfect absorption in plasmonic nanocrystal monolayers," *ACS Nano* **18**(1), 972–982 (2024). PMID: 38117550.
[40] Martinez-Cercos, D., Paulillo, B., Maniyara, R. A., Rezikyan, A., Bhattacharyya, I., Mazumder, P., and Pruneri, V., "Ultrathin metals on a transparent seed and application to infrared reflectors," *ACS Applied Materials Interfaces* **13**(39), 46990–46997 (2021).
[41] Yun, J., "Ultrathin metal films for transparent electrodes of flexible optoelectronic devices," *Advanced Functional Materials* **27**(18), 1606641 (2017).
[42] Smith, A. R., Chao, K.-J., Niu, Q., and Shih, C.-K., "Formation of atomically flat silver films on gaas with a" silver mean" quasi periodicity," *Science* **273**(5272), 226–228 (1996).
[43] Formica, N., Ghosh, D. S., Carrilero, A., Chen, T. L., Simpson, R. E., and Pruneri, V., "Ultrastable and atomically smooth ultrathin silver films grown on a copper seed layer," *ACS Applied Materials Interfaces* **5**(8), 3048–3053 (2013).
[44] Martinez-Cercos, D., Paulillo, B., Maniyara, R. A., Rezikyan, A., Bhattacharyya, I., Mazumder, P., and Pruneri, V., "Ultrathin metals on a transparent seed and application to infrared reflectors," *ACS Applied Materials Interfaces* **13**(39), 46990–46997 (2021).
[45] Sakotic, Z., Raju, A., Ware, A., Estévez H, F. A., Brown, M., Magendzo Behar, Y., Hungund, D., and Wasserman, D., "Mid-infrared perfect absorption with planar and subwavelength-perforated ultrathin metal films," *Advanced Physics Research* **3**(8), 2400012 (2024).